ACS APPLIED MATERIALS & INTERFACES

Research Article

www.acsami.org

Facile in Situ Synthesis of Silver Nanoparticles on Procyanidin-Grafted Eggshell Membrane and Their Catalytic Properties

Miao Liang,[†] Rongxin Su,*[,†,§] Renliang Huang,[‡] Wei Qi,[†,§] Yanjun Yu,[†] Libing Wang,[†] and Zhimin He[†]

[†]State Key Laboratory of Chemical Engineering, School of Chemical Engineering and Technology, Tianjin University, Tianjin 300072, P. R. China

[‡]School of Environmental Science and Engineering, Tianjin University, Tianjin 300072, P. R. China

[§]Collaborative Innovation Center of Chemical Science and Engineering (Tianjin), Tianjin 300072, P. R. China

Supporting Information

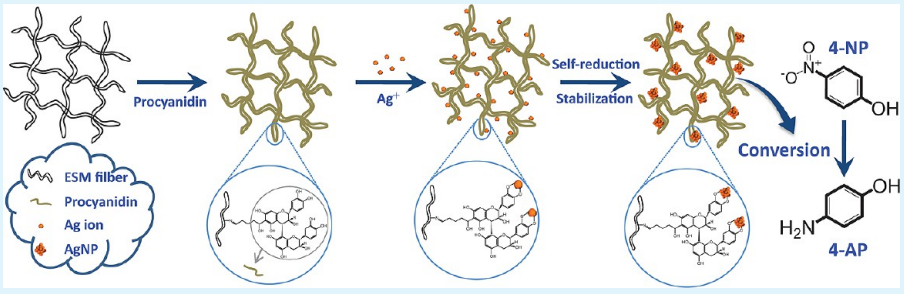

ABSTRACT: Facile, efficient, and robust immobilization of metal nanostructures on porous bioscaffolds is an interesting topic in materials chemistry and heterogeneous catalysis. This study reports a facile in situ method for the synthesis and immobilization of small silver nanoparticles (AgNPs) at room temperature on natural eggshell membrane (ESM), which presents interwoven fibrous structure and can be used as a unique protein-based biotemplate. Procyanidin (Pro), a typical plant polyphenol extracted from grape seeds and skins, was first grafted onto ESM fibers to serve as both reductant and stabilizer during the synthesis process. As a result, the AgNPs were facilely synthesized and robustly immobilized on the ESM fibers without additional chemical reductant or physical treatments. The morphology and microstructure of the as-prepared AgNPs@Pro-ESM composites were characterized by combined microscopy and spectroscopy technologies. The results indicate that small AgNPs with mean diameter of 2.46 nm were successfully prepared on the Pro-ESM biotemplate. The composites exhibited good catalytic activity toward the reduction of 4-nitrophenol (4-NP). More importantly, these composite catalysts can be easily recovered and reused for more than eight cycles because of their high stability.

KEYWORDS: *eggshell membrane, procyanidin, silver nanoparticles, catalysis, 4-nitrophenol*

INTRODUCTION

In the ever-expanding field of nanomaterials research, noble metal nanoparticles (NPs) (e.g., Au, Ag, Pt) have received considerable attention because of their fascinating physicochemical properties and remarkable potential applications in catalysis, sensing, photonics, and biomedicine.[1,2] In particular, the catalytic properties of metallic NPs are appealing to many researchers because of their high reactivity and selectivity.[3] The large surface area to volume ratio of NPs contributes to their good catalytic performance. However, nanocatalyst powders are undesirable for industrial applications because of their characteristics, such as easy aggregation, reduction in catalytic activities, and difficulty in product separation and catalysts recycling.[4−6] Therefore, it is highly desirable to design and synthesize small nanocatalyst with long-term stability for maintaining its catalytic activity during the reactions. Over the past few decades, many efforts have been devoted to developing composite catalysts by immobilizing noble metal NPs on/into solid matrix,[7−10] which appears to be an effective strategy in protecting these metal NPs against agglomeration and facilitating their recovery.

Among the various matrixes, macroscopic materials with three-dimensional (3D) interconnected porous networks are promising for the immobilization of NPs.[11−13] The porous structure endows these supports with high surface area for maximizing NP loading. For instance, Na and co-workers[14] have demonstrated that hierarchical carbon nanotube membrane can be used as support for incorporating gold NPs in the catalytic degradation of 4-nitrophenol (4-NP). In addition, polymer hydrogels have also been utilized as matrixes for the incorporation of NPs to combine the catalytic properties of nanocatalyst with the open porous structure and external stimuli-responsive characteristics of hydrogels.[15,16] Moreover, the preparation of novel composite catalysts using macroscopic biomaterials with 3D porous

Received: August 20, 2013
Accepted: March 13, 2014
Published: March 13, 2014

structure has been the focus of numerous studies. For example, Lu and our group have synthesized noble metal nanocatalysts using a chemical reduction or a biomineralization mimetic method in protein crystals that are composed of highly ordered protein assemblies with unique nanosized porous structures.[17−19] Fabrication of the above-mentioned macroscopic supports with interconnected pore networks usually involves either high temperature calcination or sophisticated manipulation (polymer cross-linking or protein crystallization), which hinders their extensive applications. Such drawbacks stimulate the exploration of new applicable and cost-effective porous supporting medium with excellent practical utility for nanocatalyst immobilization.

Eggshell membrane (ESM), a naturally available protein-based material with interwoven fibrous 3D structure, shows great promise as a novel biotemplate for immobilizing nanocatalysts. Currently, ESM has long been treated as agricultural waste and disposed in landfills without any pretreatment. However, this naturally occurring membrane possesses special characteristics, such as the ability to transport nutrients to the developing embryo and the intricate lattice network of stable protein fibers,[20] resulting in high surface area that allows high loading capacity for NPs. In recent years, fluorescent metal nanoclusters and semiconductor NPs have been successfully synthesized and immobilized on this solid matrix mainly through physical interaction.[21,22] Actually, the functional properties of these composite systems have seldom been reported, although they offer great potential applications for catalysis, chemical sensing, surface enhanced Raman scattering, and so on. This phenomenon may be caused by the fact that the NPs were physically immobilized on the ESM, and thus, the insufficient stability of NPs limits the practical applications. Our recent work also found that the weak noncovalent interaction between ESM fibers and NPs was not strong enough to maintain the stability and catalytic property of the composites during the recycling process.[23] Therefore, chemical modification of ESM fibers for improving the stability of supported NPs is desirable in order to realize the practical application of these ESM-based composites.

In this study, we prepared a surface modified and redox-active template, procyanidin-grafted ESM, for robust immobilization of silver nanoparticles (AgNPs). As efficient and cost-effective noble metal nanocatalysts, AgNPs have been applied in various catalytic reactions, such as reduction and oxidation.[24−26] The size of AgNP has a significant role on catalysis. Smaller AgNPs usually exhibit higher catalytic activity due to their greater surface to volume ratio.[6] Thus, developing effective methods for the synthesis of small and well dispersed AgNPs is necessary. Herein, procyanidin has been used, for the first time, as both reducing agent and stabilizer for the preparation of small AgNPs with sufficient dispersion. Procyanidin, a biologically active polyphenolic flavonoid, is mainly extracted from grape seeds and skins and expected to possess reducing ability toward silver or gold ions.[27,28] Previous studies have indicated that the phenolic hydroxyl groups of flavonoid compounds can chelate and reduce silver ions to metallic silver in situ.[29,30] Accordingly, procyanidin promises to be an excellent chemical that would be able to synergistically construct a stable linkage between ESM fiber and Ag^+ ions. Moreover, the utilization of procyanidin avoids the introduction of traditional organic solvents and chemical reductants, such as *N*,*N*-dimethylformamide and sodium borohydride, which are highly reactive and pose potential environmental and biological risks. Hence, this natural extracted compound can be accepted as "green" reductant for the synthesis of metallic nanoparticles.[31] Additionally, this nontoxic and facile synthesis route is compatible with the sustainable development principles.

Given the above merits of ESM and procyanidin, an efficient template was demonstrated for the facile and in situ fabrication of heterogeneous catalysts by grafting procyanidin onto the surface of the ESM fibers. The availability of synthesizing AgNPs using procyanidin was first confirmed in aqueous solution. Procyanidin was then covalently grafted onto the ESM fibers through electrophilic agent glutaraldehyde, which provides a novel template for robust immobilization of nanocatalyst. To the best of our knowledge, this study was the first to report the in situ and facile synthesis of noble metal NPs on natural ESM using a "green" reductant for catalytic application. Small AgNPs with narrow size distribution were successfully synthesized in situ on the ESM fibers by the reducing and stabilizing ability of procyanidin. The main physical and chemical properties of the as-prepared catalysts were fully characterized. Meanwhile, the catalytic performance of the composite catalysts was investigated by employing the reduction of 4-NP into 4-aminophenol (4-AP) as a model reaction. The elegance of our hybrid system is that the composite catalysts can be easily separated from the reaction mixture after the reaction, allowing the catalysts to be reused without losing their activity significantly.

EXPERIMENTAL SECTION

Materials. Grape-seed-derived procyanidin dimer (≥98%, relative molecular mass of 578.38) was generously provided by JF-Natural (Tianjin, China). Fresh membrane-bound eggshell was collected from a campus breakfast shop and immediately stored in water at 4 °C. Glutaraldehyde (50 wt %), silver nitrate ($AgNO_3$), sodium borohydride ($NaBH_4$), and 4-NP (99%) were purchased from Aladdin Reagent Company (Shanghai, China). Deionized water was used for all the experiments.

Synthesis of AgNPs in Aqueous Solution Using Procyanidin. The AgNPs were synthesized using procyanidin as both reducing and stabilizing agent. Procyanidin stock solution (10 mM) was prepared by dissolving a specific amount of procyanidin powder in deionized water. The stock solution was passed through 0.22 μm sterile filters to remove foreign nucleation sources before use. In a typical experiment, 6.8 mg of $AgNO_3$ was first dissolved in 19 mL of deionized water. Subsequently, 1 mL of procyanidin solution was rapidly added to the precursor solution under continuous stirring. The mixture was allowed to react under continuous magnetic stirring at 310 K. Samples were obtained at different reaction times and deposited into a −40 °C deep freeze refrigerator to quench the reaction until further study.

Preparation of Procyanidin Grafted Eggshell Membrane (Pro-ESM). Raw eggshells were cleaned carefully with deionized water, and the inner membrane was manually removed from the eggshell. The obtained ESM was washed thoroughly to remove the albumin, cut into small rectangular pieces (about 5 mm × 8 mm), and then dried in vacuum at room temperature for future use. In a typical procedure, a certain amount of procyanidin was dissolved in 50.0 mL of deionized water and mixed with 0.5 g of ESM pieces prepared in the previous step. The mixture was then stirred at 298 K for 2 h. Afterward, 0.5 mL of glutaraldehyde (used as cross-linking agent between ESM and procyanidin) was added into the mixture at pH 6.5, and the mixture was stirred at 310 K for 6 h. Finally, the product was collected with forceps, fully washed with water to remove the adsorbed procyanidin, and dried in vacuum to obtain the Pro-ESM.

Preparation of AgNPs@Procyanidin Grafted Eggshell Membrane Composites (AgNPs@Pro-ESM). The synthesis of supported AgNPs on Pro-ESM was ascribed to the chelating and in situ reducing capacity of procyanidin toward Ag ions. The as-prepared Pro-ESM pieces were incubated with 50 mL of $AgNO_3$ aqueous solution (10 mM) for 12 h under constant stirring at 310 K. Meanwhile, the color of Pro-ESM changed to light brown, indicating the formation of AgNPs on the

dx.doi.org/10.1021/am500665p | ACS Appl. Mater. Interfaces 2014, 6, 4638−4649

surface of the protein fibers. Afterward, the resulting AgNPs@Pro-ESM composites were again thoroughly rinsed and dried in vacuum for further analysis.

Catalytic Reduction of 4-NP. To investigate the catalytic efficiency and reusability of the AgNPs@Pro-ESM composites, reduction of 4-NP was performed according to our previously reported procedure.[19] In a typical experiment, 15 mg of AgNPs@Pro-ESM composites was added into a mixed solution containing 7 mL of deionized water and 750 μL of 4-NP (3 mM). N_2 gas was then purged through the solution for 10 min to remove the dissolved O_2. Subsequently, 1 mL of freshly prepared $NaBH_4$ solution (0.3 M) was injected under continuous stirring to initiate the reduction reaction. At each time interval, part of the mixture was transferred into a quartz cuvette, and UV−vis absorption spectra were recorded in the range 250−550 nm to monitor the catalytic reaction. The product of the catalytic reduction was also analyzed by an Agilent 1200 HPLC system using an Agilent Eclipse XDB-C18 column (150 mm × 4.6 mm, 5 μm particle size). The reaction was conducted at four temperature levels, i.e., 303.15, 308.15, 313.15, and 318.15 K, using a temperature-controlled water bath to study the effect of temperature on the catalytic property. For comparison, the control experiment was also carried out under the same experimental conditions using Pro-ESM as catalyst. The catalytic activity of the as-prepared AgNPs@Pro-ESM composites for the reduction of other nitrobenzenes (2-nitrophenol and 4-nitroaniline) was investigated.

Characterization. The growth process of AgNPs using procyanidin as reductant and stabilizer in the aqueous solution was monitored by a TU-1810 (Persee, China) UV−vis spectrophotometer. The ultraviolet−visible diffuse reflectance spectra (UV−vis DRS) of the as-prepared AgNPs@Pro-ESM composites were recorded using a Lambda 750 Perkin-Elmer UV−vis spectrophotometer equipped with an integrating sphere using $BaSO_4$ as reference. The morphological features were observed by scanning electron microscope (SEM, Hitachi S-4800) coupled with energy-dispersive X-ray spectroscopy (EDX) at an accelerating voltage of 3.0 kV. The detailed morphology and size distribution of the AgNPs were determined using a high resolution transmission electron microscope (HRTEM, JEM-2100F, 200 kV) equipped with an energy-dispersive X-ray (EDX) analysis attachment. After ultrasonication of the AgNPs@Pro-ESM composites in deionized water, a drop containing the released AgNPs was deposited onto the carbon-coated copper grids and dried at room temperature for the analysis of supported AgNPs. X-ray diffraction (XRD) measurement was carried out using D/max 2500 XRD spectrometer (Rigaku) with a Cu Kα X-ray source. X-ray photoelectron spectra (XPS, PHI-5300 ESCA, USA) of the ESM, Pro-ESM, and AgNPs@Pro-ESM were recorded with an Al Kα source ($h\nu$ = 1486.6 eV). Peaks from all of the high-resolution core spectra were fitted with XPSPEAK 4.1 software, using mixed Gaussian−Lorentzian functions. Fourier transform infrared spectroscopy (FTIR, Nicolet Nexus 670) analyses were identified within the range 400−4000 cm^{-1}. Thermogravimetric analysis (TGA) was performed using a simultaneous TGA−DTA apparatus (PTC-10A, Rigaku, Japan), from room temperature to 700 °C at a heating rate of 10 °C/min in air. The amount of AgNPs on Pro-ESM was accurately determined by inductively coupled plasma mass spectrometry (ICP-MS, Agilent 7700x, USA) after the composites were dissolved and diluted in nitric acid.

RESULTS AND DISCUSSION

Synthesis of AgNPs in Aqueous Solution Using Procyanidin. The formation of AgNPs by the reduction of $AgNO_3$ solution with grape-seed-derived procyanidin dimer was indicated by the concomitant change in the color of the reaction mixture from transparent to light brown within 12 h. The time evolution of the UV−vis spectra during the growth of AgNPs using 0.5 mM procyanidin as reductant is shown in Figure 1. At the earlier stage of the reaction (<0.5 h), the surface plasmon resonance (SPR) absorption spectrum became broad with the nucleation of Ag cluster, showing a major peak at 418 nm with low intensity. With the growth of Ag nanoparticles, the SPR peak

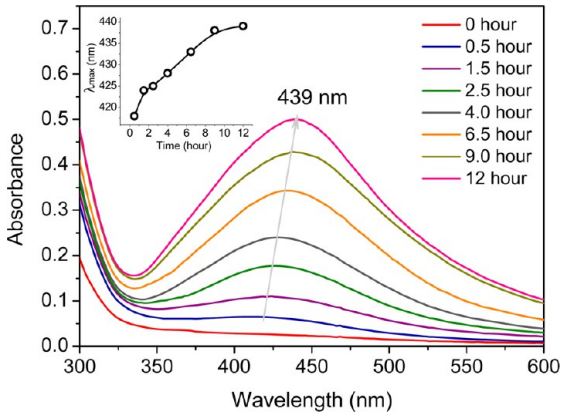

Figure 1. UV−vis absorption spectra of AgNPs synthesized in the aqueous solution at different times using procyanidin (0.5 mM).

significantly red-shifted to 439 nm after 12 h, which was accompanied by the narrowing of their bandwidths and the gradual increase in absorption intensity. This phenomenon indicates the growth process of AgNPs under the mild reducing capacity of procyanidin. According to previous literature,[28,32] this metallic Ag^+ reducing ability of plant-extracted polyphenol is attributed to the multiple hydroxyls that can chelate with the Ag^+ ions and reduce the chelated Ag^+ into Ag^0 in situ. The inset in Figure 1 shows a curve of the maximum absorption wavelength versus the reaction time. A negligible wavelength shift was observed from 9 to 12 h, suggesting that the NP size gradually stopped increasing because of the capping effect of procyanidin (TEM analysis also support this phenomenon, as shown in Figure 2 and Figure S1, Supporting Information). Therefore, a reduction reaction time of 12 h was chosen for the preparation of supported AgNPs. The SPR peak of AgNPs are influenced by their size, as well as their morphology, compositions, surface chemistry, and surrounding environment, especially for the NPs with small diameters.[33] Therefore, the morphology and size distribution of AgNPs cannot be deduced simply through the SPR peak, but they should be examined further by TEM analysis.

Figure 2 shows the typical TEM images of the AgNPs that were grown for 12 h and its corresponding size distribution histogram. The TEM results indicate that the formed small-sized NPs are predominantly spherical and well-dispersed without agglomeration in the aqueous solution (Figure 2a). Hence, procyanidin can reduce Ag^+ to AgNPs and simultaneously serve as the stabilizing agent to prevent agglomeration because of the rigid aromatic rings of molecular backbone in procyanidin. Lattice fringes are faintly visible from the further magnified HRTEM image (Figure 2b) of the AgNPs, showing the crystalline structure of AgNPs. The corresponding fast Fourier transform (FFT) pattern (Figure 2b, inset) also indicates the single crystal nature.[3] More than 200 particles in several TEM images have been analyzed using the ImageJ software to determine the size distribution. As shown in Figure 2c, the AgNPs have a narrow size distribution with an average diameter of 2.19 nm. The in situ reduction and simultaneous capping ability of procyanidin may contribute to the formation of small and uniform AgNPs.[34] These results clearly suggest that the introduction of grape-seed-derived procyanidin dimer provides a nontoxic approach for the formation of uniformly dispersed AgNPs with small particle size.

FTIR analysis was further used to investigate the structural changes of procyanidin during the synthesis process of AgNPs.

dx.doi.org/10.1021/am500665p | ACS Appl. Mater. Interfaces 2014, 6, 4638−4649

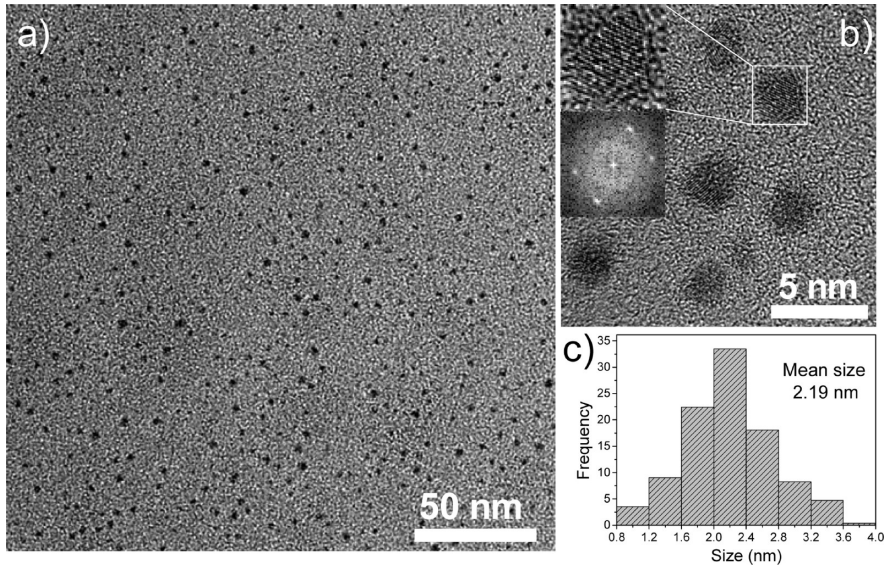

Figure 2. (a, b) TEM images of AgNPs synthesized with 0.5 mM of procyanidin in the aqueous solution. The inset in (b) shows the HRTEM image and the FFT image of a typical AgNP. (c) Histogram showing the corresponding particle size distribution of AgNPs.

The FTIR spectra of procyanidin and procyanidin-stabilized AgNPs are presented in Figure 3. An absorption peak at 3332 cm^{-1} is a characteristic of the O−H stretching vibration of phenolic hydroxyls and the methylol group. The broad range of this peak suggests the existence of hydrogen bonds among the procyanidin molecules.[28] Both samples exhibited absorption bands in the vicinity of 1640−1420 cm^{-1} (1612, 1522, and 1446 cm^{-1}), which are attributed to the aromatic rings of procyanidin. The absorption peaks at 1612, 1446, and 1105 cm^{-1} are assigned to the C=C stretching vibrations, C−H stretching vibration of the aromatic rings, and the C−O−C stretching vibration, respectively.[35] The deformation of the C−H bond vibrations in the benzene rings also provides small absorption bands in the range 910−740 cm^{-1}. The absorption peak at 1353 cm^{-1} arises from the in-plane deformation of phenolic hydroxyls (O−H bond) in procyanidin.[28] For the procyanidin-stabilized AgNPs, however, the peak for the in-plane deformation of phenolic hydroxyls shifted to 1370 cm^{-1} and became relatively narrow and weak. This change may be caused by the oxidation of phenolic hydroxyls during the formation of AgNPs. In addition, the absorption band corresponding to the stretching vibration peak of the phenolic hydroxyls shifted to 3411 cm^{-1}, which also indicated the involvement of O−H groups in the reduction of Ag^+ ions and the interaction of phenolic hydroxyls with AgNPs.[29]

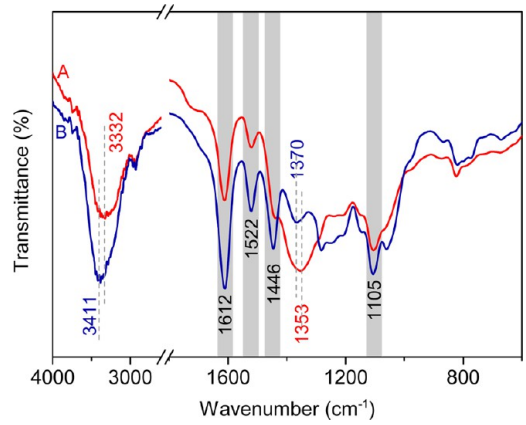

Figure 3. FTIR spectra of procyanidin before (A) and after (B) the reduction and stabilization of AgNPs.

Scheme 1. Schematic Illustration of Procyanidin Grafting and the Formation and Stabilization of AgNPs with Pro-ESM as Biotemplate

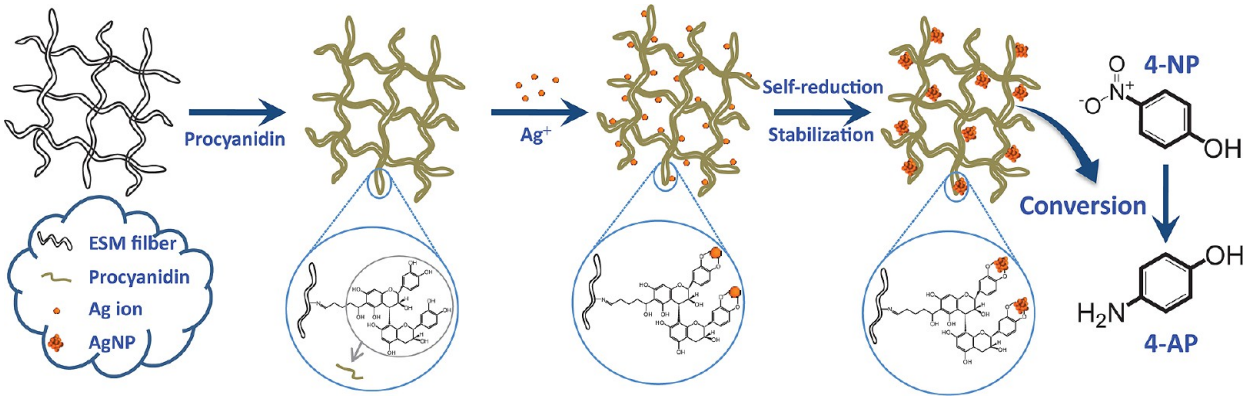

dx.doi.org/10.1021/am500665p | ACS Appl. Mater. Interfaces 2014, 6, 4638−4649

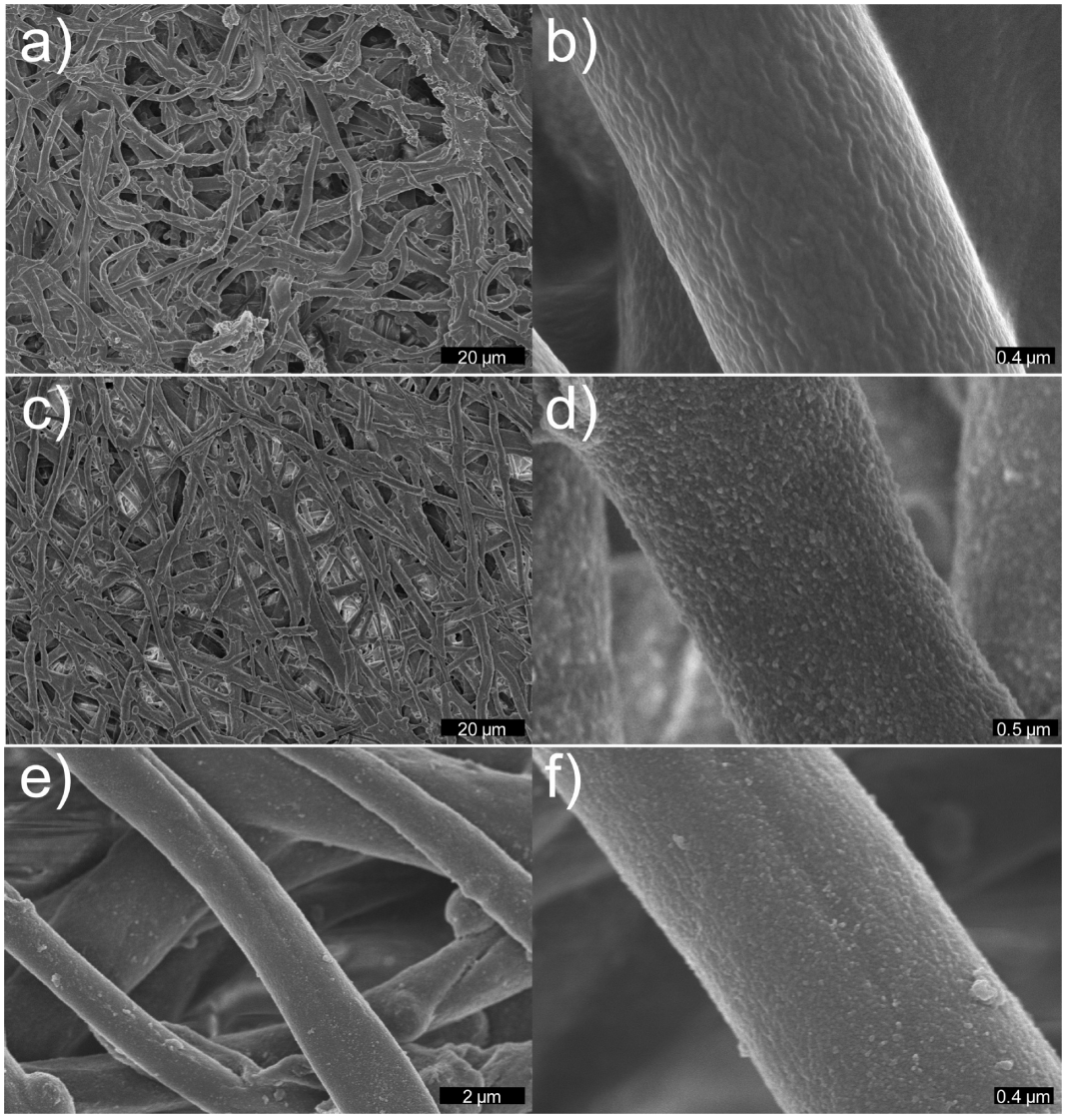

Figure 4. SEM images of natural ESM (a, b), Pro-ESM (c, d), and AgNPs@Pro-ESM (e, f) at different magnifications.

Fabrication and Characterization of AgNPs@Pro-ESM Composites. In the above work, the availability of procyanidin for synthesizing AgNPs was confirmed in an aqueous solution. As a result, small AgNPs with sufficient dispersion were successfully prepared. In the following work, we presented the fabrication of ESM-based support grafted with procyanidin and further developed an in situ growth method for preparing AgNPs@Pro-ESM composites with high catalytic activity and good recyclability.

The fabrication of the AgNPs@Pro-ESM composites is illustrated in Scheme 1. Procyanidin was grafted onto the ESM fibers using glutaraldehyde as cross-linking agent based on the following reasons. On the one hand, the ESM fibers are mainly composed of glycoproteins, such as collagen (types I, V, and X) and glycosaminoglycans. Therefore, glutaraldehyde can react with the amino groups abundantly exposed on the surface of the ESM fibers.[36] On the other hand, procyanidin dimer is composed of catechin and epicatechin. And the C6 of the A-rings of procyanidin has high nucleophilic reaction activity, which can form a covalent bond with electrophilic agents, such as aldehydes.[37] Here glutaraldehyde was used as cross-linking agent for the fabrication of Pro-ESM. And orthophenolic hydroxyls served as an excellent bidentate ligand that endows polyphenols with high affinity toward many metal ions by forming a stable five-member chelating ring.[28,38] Therefore, abundant and stable anchoring sites for Ag^+ ions can be introduced after the covalent grafting of procyanidin onto the ESM fibers. The chelated Ag^+ ions can then be spontaneously reduced into Ag^0 atoms, inducing the nucleation and growth of AgNPs in situ by the mild reduction ability of orthophenolic hydroxyls in procyanidin without any other chemical reducing agents at 37 °C. At the same time, the synthesized AgNPs are subsequently stabilized through the interaction between the surface of AgNPs and oxygen atoms of the procyanidin molecules, which may contribute to the formation of small AgNPs.[29]

SEM analysis was performed to characterize the morphology changes of ESM. Figure 4a,b shows the typical SEM images of the natural ESM at different magnifications. The biomembrane exhibited a structurally macroporous network constructed of interwoven and coalescing protein fibers with a diameter ranging from 0.5 to 2.0 μm. The high surface area caused by the intricate lattice network is beneficial to the immobilization of NPs. Meanwhile, this interconnected porous structure can endow

ESM with good permeability that allows reactants to contact the inner fibers sufficiently. After procyanidin grafting, the macroscopic hierarchical structure of ESM can be well maintained (Figure 4c). Moreover, the high magnification image of Pro-ESM presented in Figure 4d reveals that the surface of the fibers is slightly rougher than that of the natural ESM, indicating the successful grafting of procyanidin onto the fiber surface. Figure 4e,f shows the SEM photographs of the resultant AgNPs@Pro-ESM composites at different magnifications. The inherent interconnected fibrous structure of ESM is still well preserved, while the in situ synthesized AgNPs can hardly be observed, probably because of their nanosize. However, the successful formation of AgNPs on the Pro-ESM matrix can be visually witnessed by the color change of Pro-ESM from pale yellow to light brown. The EDS elemental mapping further confirmed that the Ag element was uniformly distributed on the surface of Pro-ESM (Figure S2, Supporting Information). Moreover, the immobilization of small AgNPs was further confirmed by the following XPS, UV−vis DRS, and TEM analysis.

The chemical state of silver in AgNPs@Pro-ESM composites was ascertained by XPS analysis. As shown in Figure 5a, the survey scan spectrum of AgNPs@Pro-ESM exhibits the presence of C 1s, N 1s, O 1s, Ag 3p, and Ag 3d core levels without significant impurities. Figure 5b shows the Ag 3d core-level XPS spectra of AgNPs@Pro-ESM composites. As shown in the spectrum, two peaks at 368.4 and 374.4 eV corresponded to Ag $3d_{5/2}$ and Ag $3d_{3/2}$ binding energies, respectively. The splitting of the 3d doublet of Ag is 6.0 eV, indicating the formation of metallic AgNPs (Ag^0) on the fiber surface.[3] UV−vis DRS measurement was also conducted to confirm the successful formation of AgNPs on the Pro-ESM matrix. Figure 5c presents the UV−vis DRS spectra of the natural ESM, Pro-ESM matrix, and AgNPs@Pro-ESM composites. The natural ESM possesses only two absorption bands at around 210 and 280 nm, assigned to the polypeptide chains and the aromatic groups of proteins, respectively.[39] However, after the grafting reaction, the resulting Pro-ESM matrix exhibits relatively enhanced absorption in the range 200−800 nm, corresponding to the color change of ESM from white to pale yellow. As for the spectrum of the AgNPs@Pro-ESM composites, aside from the peaks for ESM proteins, an intense absorption band with the maximum at 430 nm was observed. This band is a characteristic SPR absorption peak of AgNPs, which arises from the collective oscillation of surface conduction electrons induced by incident electromagnetic waves. And it can be influenced by particle size, morphology, surface chemistry, surrounding medium, and so on. These observations clearly indicate the in situ formation of AgNPs on the Pro-ESM matrix due to the reducing and stabilizing capacity of procyanidin.

Attenuated total reflectance fast Fourier transformation infrared spectroscopy (ATR-FTIR) was used to characterize the structural change during the grafting reaction and the in situ formation of AgNPs. As shown in Figure 6, the ATR-FTIR spectrum of natural ESM exhibited absorption bands at 1637, 1536, and 1239 cm^{-1}, which correspond to the amide I (C═O stretching vibration), amide II (N−H in plane bending vibration coupled with C−N stretching vibration), and amide III bands of the proteins in ESM, respectively.[40] The peak at 1396 cm^{-1} was assigned to the COO^- symmetric stretch from ESM proteins containing carboxyl side groups in the amino acid residues. After the grafting of procyanidin, the amide II band shifted to 1528 cm^{-1}, which might be caused by the amino groups cross-linked through glutaraldehyde. Meanwhile, the new absorption bands at

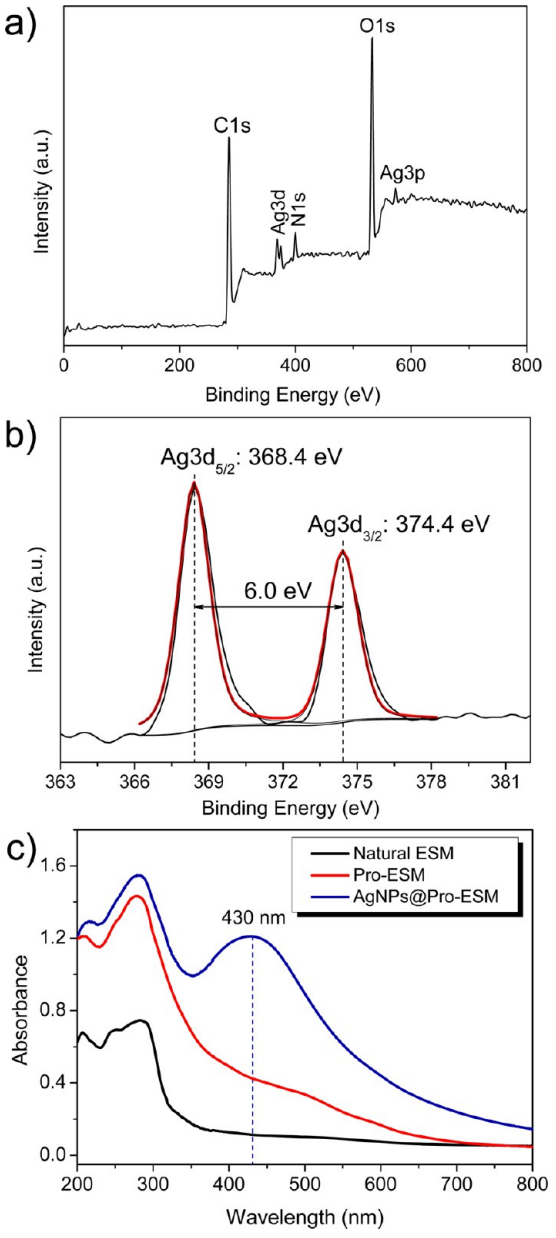

Figure 5. Survey scan (a) and Ag 3d core-level (b) XPS spectra of AgNPs@Pro-ESM composites. UV−vis DRS spectra of natural ESM, Pro-ESM, and AgNPs@Pro-ESM composites (c).

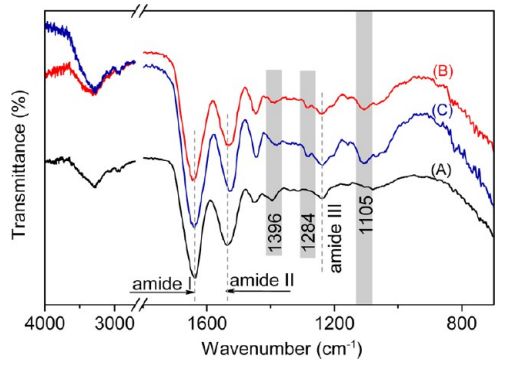

Figure 6. ATR-FTIR spectra of natural ESM (A), Pro-ESM (B), and AgNPs@Pro-ESM composites (C).

dx.doi.org/10.1021/am500665p | ACS Appl. Mater. Interfaces 2014, 6, 4638−4649

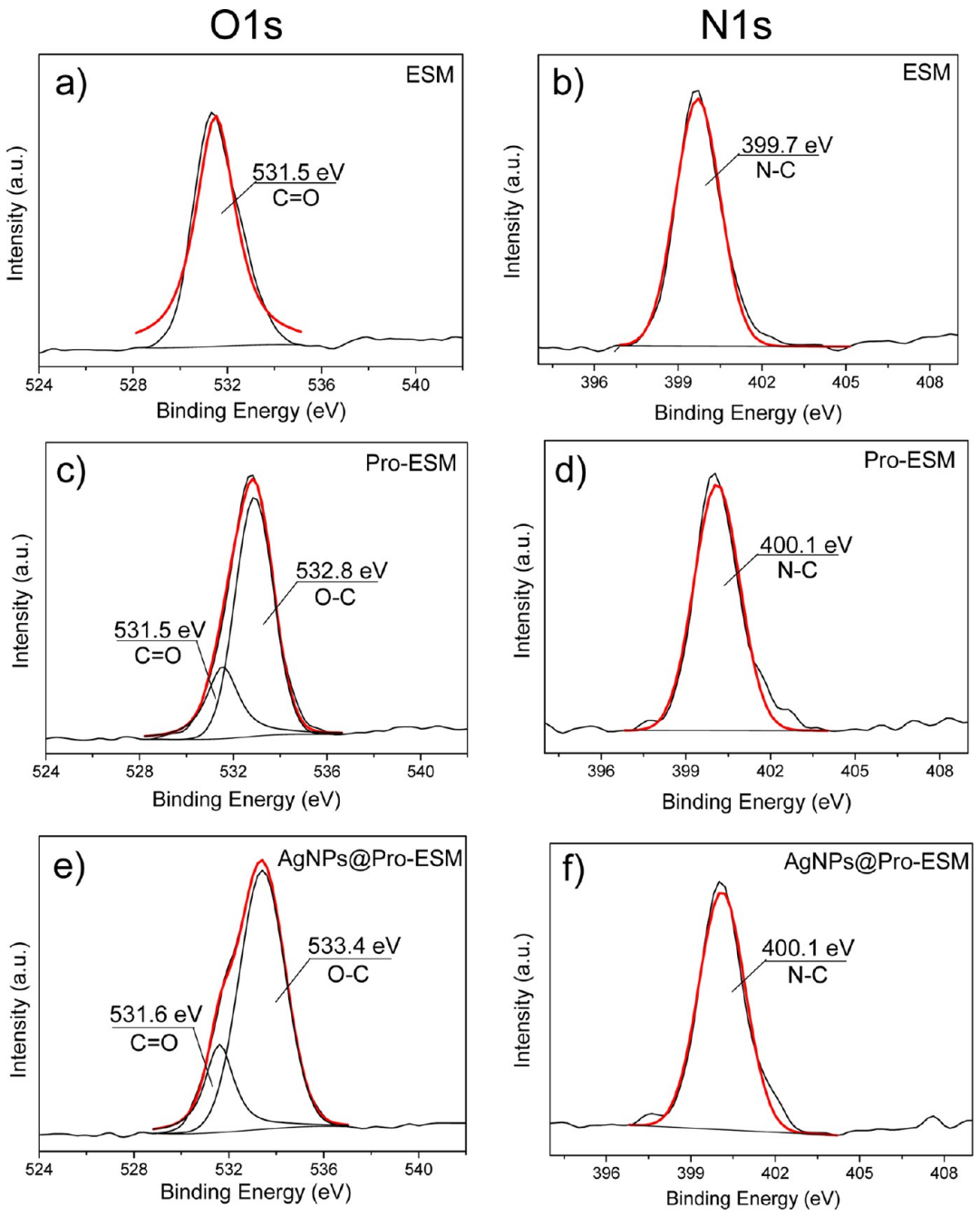

Figure 7. O 1s and N 1s core levels XPS spectra for ESM (a, b), Pro-ESM (c, d), and AgNPs@Pro-ESM composites (e, f).

1284 and 1105 cm^{-1} are ascribed to the C−O−C stretching vibration of the benzene ring in procyanidin.[29] After the in situ formation of AgNPs, the stretching vibration band of phenolic hydroxyls at 3288 cm^{-1} appeared to be relatively narrow compared with that of Pro-ESM because of the interaction of phenolic hydroxyls with AgNPs, which is consistent with the result of the synthesis of AgNPs in the aqueous solution.

In order to better understand the structure of procyanidin-grafted ESM and the interaction mechanism between AgNPs and Pro-ESM, we performed XPS analysis. The curve-fitted high-resolution XPS spectra of O 1s and N 1s core levels for ESM, Pro-ESM, and AgNPs@Pro-ESM are presented in Figure 7. Only one peak of the O 1s signal for ESM was observed at 531.5 eV, as shown in Figure 7a, which is assigned to the C═O groups in ESM. However, for Pro-ESM (Figure 7c), a new peak with higher intensity clearly appears at 532.8 eV, which is attributed to the oxygen atoms in hydroxyl groups (HO−C) of procyanidin. This result demonstrates that procyanidin was successfully grafted onto ESM fiber. This is also confirmed by the feature of the N 1s peak. As can be seen from Figure 7b and Figure 7d, the peak of N 1s (N−C) for ESM appears at 399.7 eV, which is shifted to higher binding energy (400.1 eV) after the grafting of procyanidin, suggesting a decrease of electronic density around the N atom. This is mainly due to the hydrogen bonding interactions between N atoms in polypeptide chains and H atoms in hydroxyl groups of procyanidin (C−N···HO−C).[29] As for the AgNPs@Pro-ESM composites, the peak of the HO−C group in O 1s spectra (Figure 7e) shifts from 532.8 eV to a higher binding energy of 533.4 eV, whereas no considerable change is observed for the peak of C═O groups. Meanwhile, the peak of N 1s remained almost

dx.doi.org/10.1021/am500665p | ACS Appl. Mater. Interfaces 2014, 6, 4638−4649

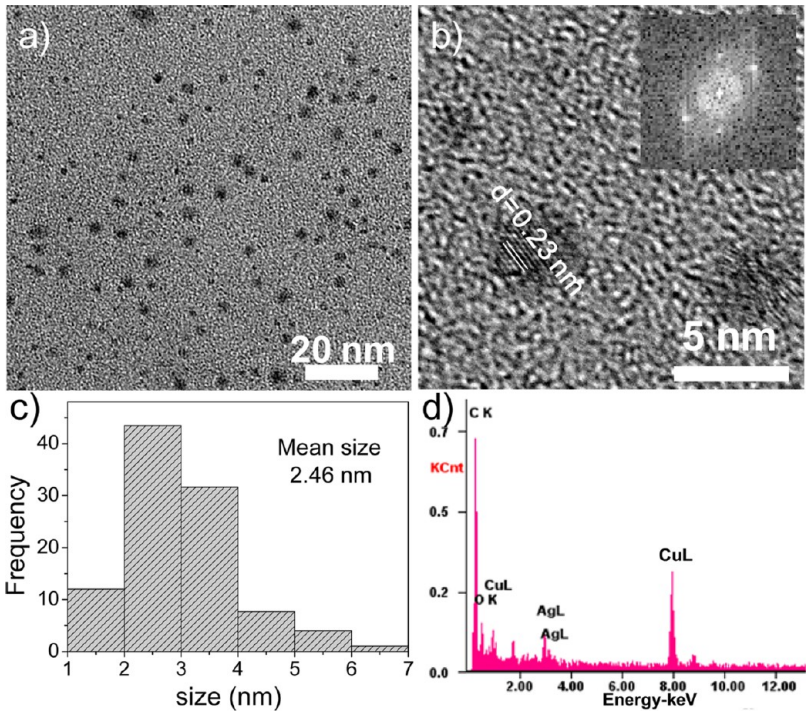

Figure 8. Typical TEM image of AgNPs released from Pro-ESM matrix under ultrasonication (a). HRTEM image of the released AgNPs and their corresponding FFT image (inset) (b). Size distribution of AgNPs synthesized on the matrix (c). EDX pattern of the supported AgNPs (d).

unchanged after the in situ formation of AgNPs (Figure 7f), indicating that the amino groups of ESM did not participate in the interaction with AgNPs. In other words, these results demonstrate that the in situ formed AgNPs are predominantly stabilized by the interaction between the surface Ag atoms of AgNPs and oxygen atoms of procyanidin.[35]

Transmission electron microscopy (TEM) measurements were carried out to characterize the morphology and size distribution of the AgNPs supported on the Pro-ESM matrix. Observing the synthesized AgNPs directly on support is difficult because the ESM is too thick to be transparent for the electron beam (Figure S3, Supporting Information). In this study, the AgNPs@Pro-ESM composites were subjected to high intensity ultrasonic waves to obtain the released AgNPs, and their representative TEM images at different magnifications are presented in Figure 8a. It can be seen that virtually spherical AgNPs with sufficient dispersion were prepared. Over 150 NPs from different images were analyzed to determine their size distribution. The corresponding histogram in Figure 8c shows that the sizes of the formed AgNPs were almost in the range 1.0−5.0 nm, with a mean diameter of 2.46 nm. Compared with those AgNPs synthesized in the aqueous solution, the diameter of the AgNPs supported on the Pro-ESM was larger and exhibited a broader size distribution. This result may be due to the heterogeneous structure of Pro-ESM during the formation of AgNPs. Despite these adverse effects, the supported AgNPs were still small enough to imply relatively high catalytic activity. A typical HRTEM image (Figure 8b) of individual AgNP and their corresponding FFT pattern (inset) shows that the nanoparticle is crystalline because the lattices of the Ag crystals can be clearly observed. The lattice fringe spacing measurements indicate that the regular lattice spacing of d = 0.23 nm is consistent with the (111) plane in the face-centered cubic (fcc) structure of the AgNPs.[3,18] In addition, the elemental composition examined by EDX (Figure 8d) exhibits the peaks for the Ag (3.0 and 3.2 keV) element, which confirmed that the NPs observed in the TEM images consist of pure Ag atoms.

The presence of single-phase AgNPs was further analyzed by XRD analysis. Figure 9a shows the corresponding XRD patterns of the natural ESM and the as-prepared Pro-ESM and AgNPs@Pro-ESM composites. All the curves showed broad signals of crystalline domains at around $2\theta = 21°$, which is ascribed to the sequence and conformations of the amino acids of the ESM proteins.[41] No other crystal diffraction peak was observed in the ESM and Pro-ESM samples. However, the Bragg reflection peaks of the AgNPs@Pro-ESM composites exhibited at 2θ of 38.1°, 44.3°, 64.5°, and 77.4° are consistent with the (111), (200), (220), and (311) crystal fcc crystalline silver, respectively (JCPDS 36-1451). In particular, these characteristic diffraction peaks are relatively weak and broadened, indicating the formation of small-sized AgNPs,[8] which is also demonstrated by HRTEM (Figure 8). Combined with the fact that all the reactions were conducted in water at 310 K in the absence of other additional reductant and stabilizers, it might be concluded that the utilization of Pro-ESM is a facile and "in situ" method for the fabrication of supported AgNPs. Therefore, a successful biomembrane platform was provided here by which small AgNPs can be synthesized and immobilized robustly onto the matrix because of the unique reducing and stabilizing properties of procyanidin. Furthermore, TGA was performed to investigate the thermal stabilities of the resulting AgNPs@Pro-ESM composites. The mass losses of the three samples before 100 °C were due to the water desorption, as shown in Figure 9b. The composite catalyst started decomposing at around 250 °C, completely decomposed at 600 °C, and exhibited a slower decomposition rate than that of natural ESM, indicating an enhanced thermal stability. The total silver content of the AgNPs@Pro-ESM composites cannot be roughly calculated from the difference in weight loss due to the impurities (mainly Si, Ca, K) in ESM.[23] We further conducted ICP-MS analysis to

dx.doi.org/10.1021/am500665p | ACS Appl. Mater. Interfaces 2014, 6, 4638−4649

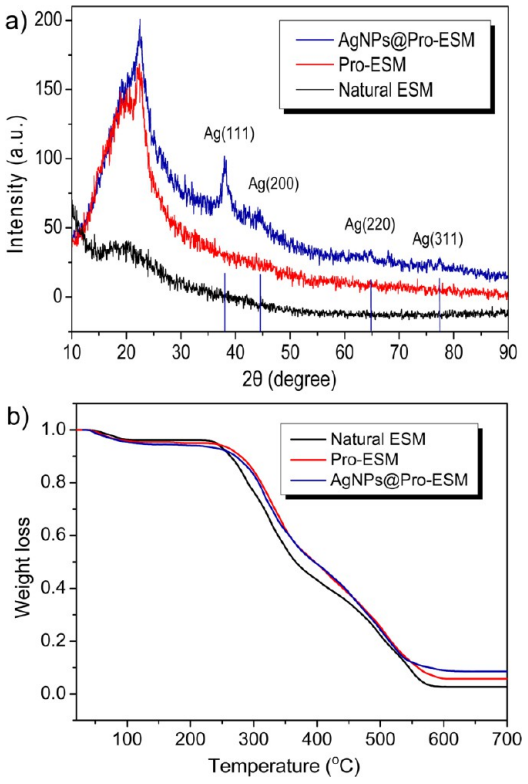

Figure 9. XRD patterns of natural ESM, Pro-ESM, and AgNPs@Pro-ESM composites (a). TGA curves for samples of ESM, Pro-ESM, and AgNPs@Pro-ESM composites heated at 10 °C min^{-1} from room temperature to 700 °C in air (b).

determine the total silver content. The result shows that the content of Ag in AgNPs@Pro-ESM composites is approximately 1.8%.

Catalytic Properties of AgNPs@Pro-ESM. 4-NP has attracted great public concern because it can cause water pollution, while its derivative, 4-AP, is a potent industrial intermediate for analgesic and antipyretic drugs, photographic developers, anticorrosion lubricants, and so on.[19] In this study, the reduction of 4-NP to 4-AP in the presence of $NaBH_4$ was chosen as a target reaction to quantitatively evaluate the heterogeneous catalytic properties of the as-prepared AgNPs@Pro-ESM catalysts.[42−45]

Although the reduction of 4-NP to 4-Ap is thermodynamically downhill (E_0|4-NP/4-AP = −0.76 V, $E_0|H_3BO_3/BH_4^-$ = −1.33 V versus normal hydrogen electrode), this process does not proceed without catalysts because of the kinetic barrier caused by the large potential difference between the donor and the acceptor molecules. In this respect, metal nanocatalysts can catalyze the reaction by acting as an electronic relay agent to overcome the kinetic barrier, allowing the electron transfer from BH_4^- to 4-NP.[46] Figure 10a presents the time-dependent evolution of the UV−vis spectra of this reaction with AgNPs@Pro-ESM composites as catalyst, showing a successive intensity decrease in the absorption peak at 400 nm, along with a concomitant appearance of a new peak at about 300 nm. Generally, the original 4-NP solution shows an absorbance peak at 317 nm under neutral conditions, which shifts to 400 nm after adding $NaBH_4$ because of the formation of 4-nitrophenolate ions via deprotonation (pK_a = 7.2).[14] During the reduction of 4-NP to 4-AP, the intensity of the absorption peak at 400 nm gradually decreased because of the consumption of substrate (4-NP), resulting in the fading and ultimate bleaching of the yellow-green color of 4-nitrophenolate. Meanwhile, the generation of reduction product 4-AP led to a new UV−vis peak at approximately 300 nm.[47] Moreover, as shown in Figure 10a, all the spectra intersect each other at two points, indicating that the nitro compound was gradually converted to 4-AP without the formation of byproducts.[18] After a 1200 s reaction, the peak at 400 nm ascribed to 4-nitrophenolate disappeared, indicating the complete transformation of the 4-NP. The formation of 4-AP was further confirmed by comparing the HPLC elution profile of reaction product with authentic 4-AP (Figure S4, Supporting Information). Meanwhile, at the end of the reaction, the peak for 4-NP almost disappeared and only the peak for 4-AP could be observed at an elution time of 4.5 min, thus suggesting the presence of product with high purity. Additionally, the control experiment was performed by taking Pro-ESM instead of AgNPs@Pro-ESM. In this case, the intensity of the peak at 400 nm remained unchanged even after 4 h, confirming the catalytic role of immobilized AgNPs on the reduction reaction.

Given that the concentration of $NaBH_4$ significantly exceeds that of 4-NP in the reaction system, the reduction rate was roughly independent of $NaBH_4$ concentration. Generally, the kinetics can be considered as pseudo-first-order with respect to 4-NP.[15] In this case, the consumption of 4-NP is given by

$$-r_t = \frac{-\mathrm{d}C_t}{\mathrm{d}t} = kC_t \quad (1)$$

where r_t is the consumption rate of 4-NP at time t, C_t is the concentration of 4-NP at time t, and k is the first-order rate constant.

Figure 10b shows the C_t/C_0 and $\ln(C_t/C_0)$ versus reaction time for the reduction of 4-NP using the AgNPs@Pro-ESM composites as catalyst. In this work, C_t/C_0 was obtained from the relative intensity of the absorption at 400 nm because the absorption intensity of 4-NP is proportional to its concentration in the medium. The linear relationship between $\ln(C_t/C_0)$ and reaction time (t) confirms the pseudo-first-order kinetics. The rate constant (k) of the catalytic reaction was 0.175 min^{-1} (2.92×10^{-3} s^{-1}) from the slope of the linear plot. The rate constants of various matrix-supported AgNPs under the different reaction conditions are presented in Table S1 for comparison (see Supporting Information). On the basis of the ICP-MS analysis as mentioned before, the ratio of the rate constant to the catalyst weight was 10.8 s^{-1} g^{-1}, indicating the high activity of AgNPs@Pro-ESM composites. The activity is much higher than that of AgNP-doped carbon sphere (1.69 s^{-1} g^{-1}) and AgNP-supported halloysite nanotubes (0.087 s^{-1} g^{-1}).[48,49] Generally, the rate constant of catalytic reaction is affected by the concentration or loading amount of nanocrystals. For example, the reaction can be completed in 660 s in the presence of more AgNPs@Pro-ESM composites (20 mg, Figure S5, Supporting Information), indicating a significant effect of the amount of catalyst on reaction rate. In this study, Ag nanocatalysts with small size (2.46 nm) in AgNPs@Pro-ESM may contribute to the high catalytic activity, since they possess much greater specific surface area and thus more atoms on the surface as potential catalytic sites.[6] In addition, the interconnected macroporous network of ESM and in situ growth (without aggregation) of AgNPs allowed 4-nitrophenolate ions to contact the supported AgNPs effectively.

As we know, the operating stability of AgNPs@Pro-ESM that influences the catalytic and recycling performance is a key point for success. In this work, the recycling and reuse of AgNPs@Pro-ESM were further examined under the same reaction conditions

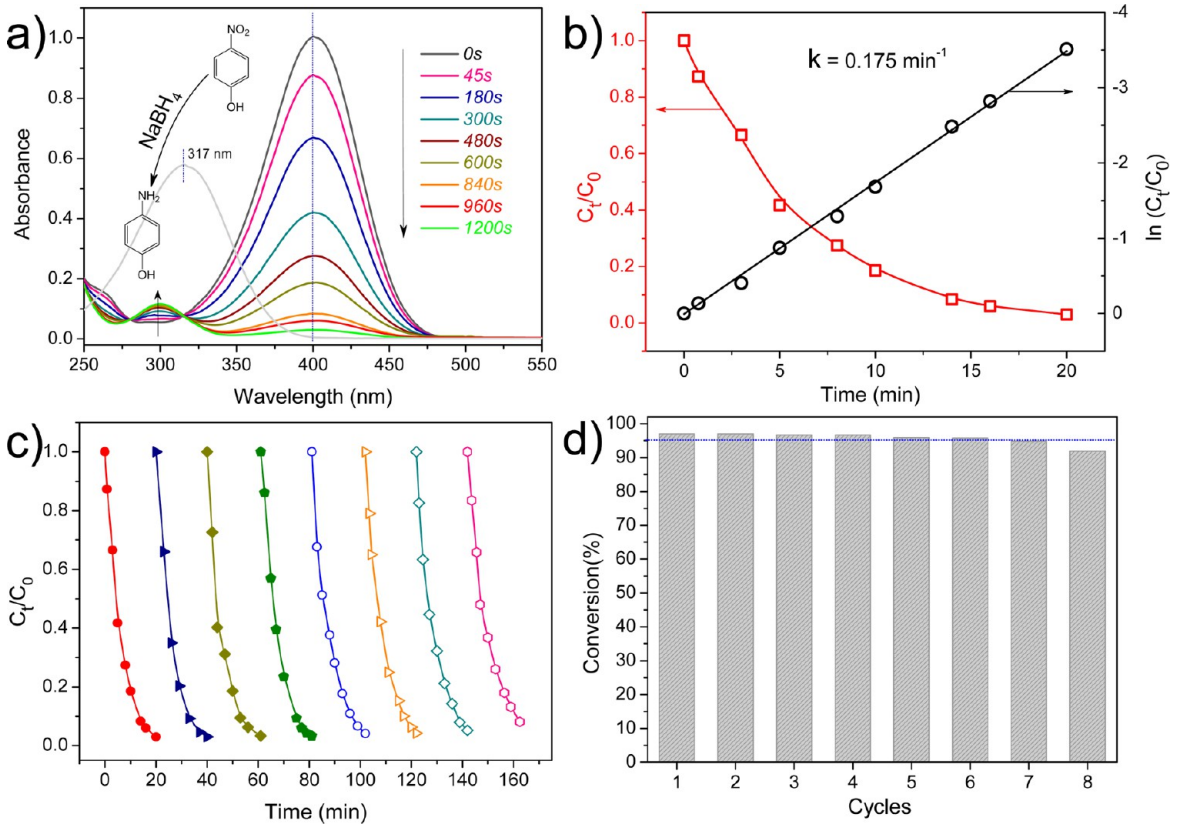

Figure 10. Catalytic performance of the AgNPs@Pro-ESM composite catalysts. Time-dependent UV−vis spectral changes (a) and the kinetic curve (b) for the catalytic reduction of 4-NP to 4-AP at 308.15 K. Recycling and reuse of AgNPs@Pro-ESM composite for the reduction of 4-NP to 4-AP (c). Conversion efficiency of 4-NP in eight successive cycles (d).

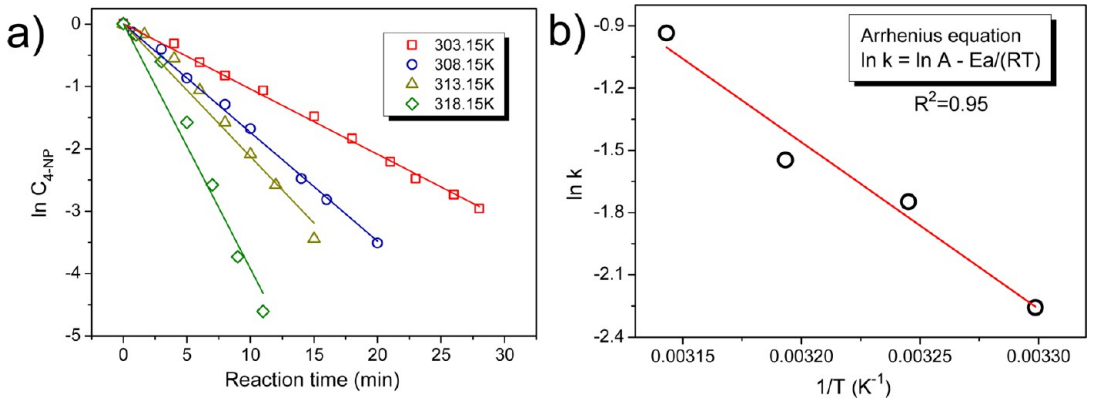

Figure 11. Effect of reaction temperature on the reduction rate (a). Arrhenius plots of ln(k) versus $1/T$ for the reduction reaction at 303.15, 308.15, 313.15, and 318.15 K (b).

as that of the first cycle. As shown in Figure 10c,d, AgNPs@Pro-ESM retained 92% productivity after eight cycles, suggesting the high stability and excellent recyclability. The good recyclability of AgNPs@Pro-ESM should be attributed to the strong stabilization ability of procyanidin toward the synthesized small AgNPs. These results clearly demonstrate that the Pro-ESMs are excellent supporting carrier for AgNPs growth and immobilization because of their physical robustness, high specific surface area, and interwoven fibrous 3D structure properties. The AgNPs@Pro-ESM can be also used for the reduction of other nitrobenzene analogues such as 2-nitrophenol and 4-nitroaniline (Figure S6, Supporting Information).

The effect of reaction temperature on the reduction rate was finally examined. As shown in Figure 11a, the corresponding linear relationship between $\ln(C_t/C_0)$ and reaction time is found at different temperatures. The rate constants of the catalytic reaction were determined from the slope of the time courses. A classic Arrhenius theory was applied to the data to obtain the activation energies. The Arrhenius equation is shown as follows:

$$\ln k = \ln A - \frac{E_a}{RT} \quad (2)$$

where k is the first-order rate constant, A is the pre-exponential factor, E_a is the activation energy, R is the universal gas constant, and T is the reaction temperature.

dx.doi.org/10.1021/am500665p | ACS Appl. Mater. Interfaces 2014, 6, 4638−4649

On the basis of the linear fitting of ln k versus $1/T$, the activation energies were determined as 66.8 kJ/mol from the slope. The E_a value in our work differs appreciably from that in some groups,[50] which may be attributed to the different surface properties and immobilizing methods of the Ag nanocatalysts. Generally, E_a is an empirical parameter for all chemical reactions, which reflects the temperature dependency of the kinetic constant. The relatively larger E_a value indicates that the kinetic constant k is more sensitive to reaction temperature in the AgNPs@Pro-ESM catalytic system.

CONCLUSIONS

This study had demonstrated that procyanidin-grafted natural ESM could be utilized as excellent carrier for the facile in situ synthesis of well-dispersed small AgNPs. Procyanidin serves as both reductant and stabilizer in the preparation process, thereby avoiding the introduction of other additional reducing agents or physical treatments. The synthesized AgNPs showed enhanced structural stability due to the high affinity of NPs onto phenolic hydroxyls of procyanidin, which was chemically grafted onto the ESM fibers. Furthermore, the as-prepared AgNPs@Pro-ESM composites exhibited good catalytic activity and high reusability for the reduction of 4-NP. Given the interwoven fibrous structure, abundant functional groups, and physical robustness of Pro-ESM, in situ synthesis and immobilization of NPs onto Pro-ESM show promising applications as facile, cost-effective, environment-friendly composite catalysts for heterogeneous catalysis.

ASSOCIATED CONTENT

Supporting Information

TEM images of AgNPs, EDS mapping of Ag element, TEM image for composites, catalytic reaction monitored by HPLC, comparison of rate constants of supported AgNPs, UV−vis spectral changes of 4-NP reduction using 20 mg of catalyst, and catalytic reduction of other nitrobenzene analogues. This material is available free of charge via the Internet at http://pubs.acs.org.

AUTHOR INFORMATION

Corresponding Author

*E-mail: surx@tju.edu.cn. Phone: +86 22 27407799. Fax: +86 22 27407599.

Notes

The authors declare no competing financial interest.

ACKNOWLEDGMENTS

This work was supported by the Ministry of Science and Technology of China (Grants 2012AA06A303, 2012YQ090194, and 2012BAD29B05), the Natural Science Foundation of China (Grants 21276192, 51173128, and 31071509), and the Ministry of Education (Grants B06006 and NCET-11-0372).

REFERENCES

(1) Cobley, C. M.; Chen, J.; Cho, E. C.; Wang, L. V.; Xia, Y. Gold Nanostructures: A Class of Multifunctional Materials for Biomedical Applications. *Chem. Soc. Rev.* **2011**, *40*, 44−56.

(2) Zou, L.; Qi, W.; Huang, R.; Su, R.; Wang, M.; He, Z. Green Synthesis of a Gold Nanoparticle−Nanocluster Composite Nanostructures Using Trypsin as Linking and Reducing Agents. *ACS Sustainable Chem. Eng.* **2013**, *1*, 1398−1404.

(3) Zhang, P.; Shao, C.; Zhang, Z.; Zhang, M.; Mu, J.; Guo, Z.; Liu, Y. In Situ Assembly of Well-Dispersed Ag Nanoparticles (AgNPs) on Electrospun Carbon Nanofibers (CNFs) for Catalytic Reduction of 4-Nitrophenol. *Nanoscale* **2011**, *3*, 3357−3363.

(4) Yang, M.; Pan, X.; Zhang, N.; Xu, Y. A Facile One-Step Way To Anchor Noble Metal (Au, Ag, Pd) Nanoparticles on a Reduced Graphene Oxide Mat with Catalytic Activity for Selective Reduction of Nitroaromatic Compounds. *CrystEngComm* **2013**, *15*, 6819−6828.

(5) Xiao, F. Layer-by-Layer Self-Assembly Construction of Highly Ordered Metal-TiO_2 Nanotube Arrays Heterostructures (M/TNTs, M = Au, Ag, Pt) with Tunable Catalytic Activities. *J. Phys. Chem. C* **2012**, *116*, 16487−16498.

(6) Zhang, Z.; Shao, C.; Sun, Y.; Mu, J.; Zhang, M.; Zhang, P.; Guo, Z.; Liang, P.; Wang, C.; Liu, Y. Tubular Nanocomposite Catalysts Based on Size-Controlled and Highly Dispersed Silver Nanoparticles Assembled on Electrospun Silica Nanotubes for Catalytic Reduction of 4-Nitrophenol. *J. Mater. Chem.* **2012**, *22*, 1387−1395.

(7) Hao, Y.; Chong, Y.; Li, S.; Yang, H. Controlled Synthesis of Au Nanoparticles in the Nanocages of SBA-16: Improved Activity and Enhanced Recyclability for the Oxidative Esterification of Alcohols. *J. Phys. Chem. C* **2012**, *116*, 6512−6519.

(8) Jiang, H.-L.; Akita, T.; Ishida, T.; Haruta, M.; Xu, Q. Synergistic Catalysis of Au@Ag Core−Shell Nanoparticles Stabilized on Metal−Organic Framework. *J. Am. Chem. Soc.* **2011**, *133*, 1304−1306.

(9) Zheng, Y.; Wang, A. Ag Nanoparticle-Entrapped Hydrogel as Promising Material for Catalytic Reduction of Organic Dyes. *J. Mater. Chem.* **2012**, *22*, 16552−16559.

(10) Adhikari, B.; Biswas, A.; Banerjee, A. Graphene Oxide-Based Hydrogels To Make Metal Nanoparticle-Containing Reduced Graphene Oxide-Based Functional Hybrid Hydrogels. *ACS Appl. Mater. Interfaces* **2012**, *4*, 5472−5482.

(11) Liang, M.; Jin, F.; Liu, R.; Yu, Y.; Su, R.; Wang, L.; Qi, W.; He, Z. Shape Evolution and Thermal Stability of Lysozyme Crystals: Effect of pH and Temperature. *Bioprocess Biosyst. Eng.* **2013**, *36*, 91−99.

(12) Wu, Z.; Sun, Y.; Tan, Y.; Yang, S.; Feng, X.; Muellen, K. Three-Dimensional Graphene-Based Macro- and Mesoporous Frameworks for High-Performance Electrochemical Capacitive Energy Storage. *J. Am. Chem. Soc.* **2012**, *134*, 19532−19535.

(13) Son, H. Y.; Ryu, J. H.; Lee, H.; Nam, Y. S. Bioinspired Templating Synthesis of Metal−Polymer Hybrid Nanostructures within 3D Electrospun Nanofibers. *ACS Appl. Mater. Interfaces* **2013**, *5*, 6381−6390.

(14) Wang, H.; Dong, Z.; Na, C. Hierarchical Carbon Nanotube Membrane-Supported Gold Nanoparticles for Rapid Catalytic Reduction of *p*-Nitrophenol. *ACS Sustainable Chem. Eng.* **2013**, *1*, 746−752.

(15) Zhu, C.; Hai, Z.; Cui, C.; Li, H.; Chen, J.; Yu, S. In Situ Controlled Synthesis of Thermosensitive Poly(*N*-isopropylacrylamide)/Au Nanocomposite Hydrogels by Gamma Radiation for Catalytic Application. *Small* **2012**, *8*, 930−936.

(16) Ai, L.; Yue, H.; Jiang, J. Environmentally Friendly Light-Driven Synthesis of Ag Nanoparticles in Situ Grown on Magnetically Separable Biohydrogels as Highly Active and Recyclable Catalysts for 4-Nitrophenol Reduction. *J. Mater. Chem.* **2012**, *22*, 23447−23453.

(17) Wei, H.; Lu, Y. Catalysis of Gold Nanoparticles within Lysozyme Single Crystals. *Chem.—Asian J.* **2012**, *7*, 680−683.

(18) Liang, M.; Wang, L.; Su, R.; Qi, W.; Wang, M.; Yu, Y.; He, Z. Synthesis of Silver Nanoparticles within Cross-Linked Lysozyme Crystals as Recyclable Catalysts for 4-Nitrophenol Reduction. *Catal. Sci. Technol.* **2013**, *3*, 1910−1914.

(19) Liang, M.; Wang, L.; Liu, X.; Qi, W.; Su, R.; Huang, R.; Yu, Y.; He, Z. Cross-Linked Lysozyme Crystal Templated Synthesis of Au Nanoparticles as High-Performance Recyclable Catalysts. *Nanotechnology* **2013**, *24*, 245601.

(20) Tsai, W. T.; Yang, J. M.; Lai, C. W.; Cheng, Y. H.; Lin, C. C.; Yeh, C. W. Characterization and Adsorption Properties of Eggshells and Eggshell Membrane. *Bioresour. Technol.* **2006**, *97*, 488−493.

(21) Shao, C.; Yuan, B.; Wang, H.; Zhou, Q.; Li, Y.; Guan, Y.; Deng, Z. Eggshell Membrane as a Multimodal Solid State Platform for Generating Fluorescent Metal nanoclusters. *J. Mater. Chem.* **2011**, *21*, 2863−2866.

(22) Su, H.; Han, J.; Wang, N.; Dong, Q.; Zhang, D.; Zhang, C. In Situ Synthesis of Lead Sulfide Nanoclusters on Eggshell Membrane Fibers by an Ambient Bio-Inspired Technique. *Smart Mater. Struct.* **2008**, *17*, 015045.
(23) Liang, M.; Su, R.; Qi, W.; Yu, Y.; Wang, L.; He, Z. Synthesis of Well-Dispersed Ag Nanoparticles on Eggshell Membrane for Catalytic Reduction of 4-Nitrophenol. *J. Mater. Sci.* **2014**, *49*, 1639−1647.
(24) Dai, J.; Bruening, M. L. Catalytic Nanoparticles Formed by Reduction of Metal Ions in Multilayered Polyelectrolyte Films. *Nano Lett.* **2002**, *2*, 497−501.
(25) Han, J.; Fang, P.; Jiang, W.; Li, L.; Guo, R. Ag-Nanoparticle-Loaded Mesoporous Silica: Spontaneous Formation of Ag Nanoparticles and Mesoporous Silica SBA-15 by a One-Pot Strategy and Their Catalytic Applications. *Langmuir* **2012**, *28*, 4768−4775.
(26) Yang, G.; Gao, G.; Wang, C.; Xu, C.; Li, H. Controllable Deposition of Ag Nanoparticles on Carbon Nanotubes as a Catalyst for Hydrazine Oxidation. *Carbon* **2008**, *46*, 747−752.
(27) Liang, M.; Liu, R.; Qi, W.; Su, R.; Yu, Y.; Wang, L.; He, Z. Interaction between Lysozyme and Procyanidin: Multilevel Structural Nature and Effect of Carbohydrates. *Food Chem.* **2013**, *138*, 1596−1603.
(28) Huang, X.; Wu, H.; Liao, X.; Shi, B. One-Step, Size-Controlled Synthesis of Gold Nanoparticles at Room Temperature Using Plant Tannin. *Green Chem.* **2010**, *12*, 395−399.
(29) Bulut, E.; Ozacar, M. Rapid, Facile Synthesis of Silver Nanostructure Using Hydrolyzable Tannin. *Ind. Eng. Chem. Res.* **2009**, *48*, 5686−5690.
(30) Guo, J.; Wu, H.; Liao, X.; Shi, B. Facile Synthesis of Size-Controlled Silver Nanoparticles Using Plant Tannin Grafted Collagen Fiber as Reductant and Stabilizer for Microwave Absorption Application in the Whole Ku Band. *J. Phys. Chem. C* **2011**, *115*, 23688−23694.
(31) Moulton, M. C.; Braydich-Stolle, L. K.; Nadagouda, M. N.; Kunzelman, S.; Hussain, S. M.; Varma, R. S. Synthesis, Characterization and Biocompatibility of "Green" Synthesized Silver Nanoparticles using Tea Polyphenols. *Nanoscale* **2010**, *2*, 763−770.
(32) Dadosh, T. Synthesis of Uniform Silver Nanoparticles with a Controllable Size. *Mater. Lett.* **2009**, *63*, 2236−2238.
(33) Peng, S.; McMahon, J. M.; Schatz, G. C.; Gray, S. K.; Sun, Y. Reversing the Size-Dependence of Surface Plasmon Resonances. *Proc. Natl. Acad. Sci. U.S.A.* **2010**, *107*, 14530−14534.
(34) Zou, M.; Du, M.; Zhu, H.; Xu, C.; Li, N.; Fu, Y. Synthesis of Silver Nanoparticles in Electrospun Polyacrylonitrile Nanofibers Using Tea Polyphenols as the Reductant. *Polym. Eng. Sci.* **2013**, *53*, 1099−1108.
(35) Zhu, H.; Du, M.; Zou, M.; Xu, C.; Li, N.; Fu, Y. Facile and Green Synthesis of Well-Dispersed Au Nanoparticles in PAN Nanofibers by Tea Polyphenols. *J. Mater. Chem.* **2012**, *22*, 9301−9307.
(36) Yang, D.; Qi, L.; Ma, J. Eggshell Membrane Templating of Hierarchically Ordered Macroporous Networks Composed of TiO_2 Tubes. *Adv. Mater.* **2002**, *14*, 1543−1546.
(37) Huang, X.; Wang, Y.; Liao, X.; Shi, B. Adsorptive Recovery of Au^{3+} from Aqueous Solutions Using Bayberry Tannin-Immobilized Mesoporous Silica. *J. Hazard. Mater.* **2010**, *183*, 793−798.
(38) Liao, X.; Zhang, M.; Shi, B. Collagen-Fiber-Immobilized Tannins and Their Adsorption of Au(III). *Ind. Eng. Chem. Res.* **2004**, *43*, 2222−2227.
(39) Guo, J.; Wang, X.; Liao, X.; Zhanga, W.; Shi, B. Skin Collagen Fiber-Biotemplated Synthesis of Size-Tunable Silver Nanoparticle-Embedded Hierarchical Intertextures with Lightweight and Highly Efficient Microwave Absorption Properties. *J. Phys. Chem. C* **2012**, *116*, 8188−8195.
(40) Guli, M.; Lambert, E. M.; Li, M.; Mann, S. Template-Directed Synthesis of Nanoplasmonic Arrays by Intracrystalline Metalization of Cross-Linked Lysozyme Crystals. *Angew. Chem.* **2010**, *122*, 530−533.
(41) Su, H.; Xu, J.; Chen, J.; Moon, W.; Zhang, D. In Situ Formation and Assembly of CdS Nanocrystallites into Polyhedrons on Eggshell Membrane at Room Temperature. *Appl. Phys. A: Mater. Sci. Process.* **2012**, *106*, 93−97.
(42) Lu, P.; Xia, Y. Novel Nanostructures of Rutile Fabricated by Templating against Yarns of Polystyrene Nanofibrils and Their Catalytic Applications. *ACS Appl. Mater. Interfaces* **2013**, *5*, 6391−6399.
(43) Yang, M.; Weng, B.; Xu, Y. Improving the Visible Light Photoactivity of In_2S_3−Graphene Nanocomposite via a Simple Surface Charge Modification Approach. *Langmuir* **2013**, *29*, 10549−10558.
(44) Chen, Z.; Liu, S.; Yang, M.; Xu, Y. Synthesis of Uniform CdS Nanospheres/Graphene Hybrid Nanocomposites and Their Application as Visible Light Photocatalyst for Selective Reduction of Nitro Organics in Water. *ACS Appl. Mater. Interfaces* **2013**, *5*, 4309−4319.
(45) Liu, S.; Chen, Z.; Zhang, N.; Tang, Z.; Xu, Y. An Efficient Self-Assembly of CdS Nanowires—Reduced Graphene Oxide Nanocomposites for Selective Reduction of Nitro Organics under Visible Light Irradiation. *J. Phys. Chem. C* **2013**, *117*, 8251−8261.
(46) Gangula, A.; Podila, R.; Ramakrishna, M.; Karanam, L.; Janardhana, C.; Rao, A. M. Catalytic Reduction of 4-Nitrophenol Using Biogenic Gold and Silver Nanoparticles Derived from Breynia Rhamnoides. *Langmuir* **2011**, *27*, 15268−15274.
(47) Liu, C.; Chen, X.; Hu, Y.; Sham, T.; Sun, Q.; Chang, J.; Gao, X.; Sun, X.; Wang, S. One-Pot Environmentally Friendly Approach toward Highly Catalytically Active Bimetal-Nanoparticle-Graphene Hybrids. *ACS Appl. Mater. Interfaces* **2013**, *5*, 5072−5079.
(48) Tang, S.; Vongehr, S.; Meng, X. Carbon Spheres with Controllable Silver Nanoparticle Doping. *J. Phys. Chem. C* **2009**, *114*, 977−982.
(49) Liu, P.; Zhao, M. Silver Nanoparticle Supported on Halloysite Nanotubes Catalyzed Reduction of 4-Nitrophenol (4-NP). *Appl. Surf. Sci.* **2009**, *255*, 3989−3993.
(50) Wunder, S.; Polzer, F.; Lu, Y.; Mei, Y.; Ballauff, M. Kinetic Analysis of Catalytic Reduction of 4-Nitrophenol by Metallic Nanoparticles Immobilized in Spherical Polyelectrolyte Brushes. *J. Phys. Chem. C* **2010**, *114*, 8814−8820.